

Foundations of Space-Time Finite Element Methods: Polytopes, Interpolation, and Integration

Cory V. Frontin

*Department of Aeronautics and Astronautics, Massachusetts Institute of Technology,
Cambridge, Massachusetts 02139*

Gage S. Walters

*Department of Mechanical Engineering, The Pennsylvania State University, University
Park, Pennsylvania 16802*

Freddie D. Witherden

Department of Ocean Engineering, Texas A&M University, College Station, Texas 77843

Carl W. Lee

Department of Mathematics, University of Kentucky, Lexington, Kentucky 40506

David M. Williams*

*Department of Mechanical Engineering, The Pennsylvania State University, University
Park, Pennsylvania 16802*

David L. Darmofal

*Department of Aeronautics and Astronautics, Massachusetts Institute of Technology,
Cambridge, Massachusetts 02139*

Abstract

The main purpose of this article is to facilitate the implementation of space-time finite element methods in four-dimensional space. In order to develop a finite element method in this setting, it is necessary to create a numerical foundation, or equivalently a numerical infrastructure. This foundation should include a collection of suitable elements (usually hypercubes, simplices, or closely related polytopes), numerical interpolation procedures (usually orthonormal polynomial bases), and numerical integration procedures (usually quadrature rules). It is well known that each of these areas has yet to be fully explored, and in the present article, we attempt to directly address this issue. We begin by developing a concrete, sequential procedure for constructing generic four-

*Corresponding author

Email address: david.m.williams@psu.edu (David M. Williams)

dimensional elements (4-polytopes). Thereafter, we review the key numerical properties of several canonical elements: the tesseract, tetrahedral prism, and pentatope. Here, we provide explicit expressions for orthonormal polynomial bases on these elements. Next, we construct fully symmetric quadrature rules with positive weights that are capable of exactly integrating high-degree polynomials, e.g. up to degree 17 on the tesseract. Finally, the quadrature rules are successfully tested using a set of canonical numerical experiments on polynomial and transcendental functions.

Keywords: space-time; finite element methods; quadrature; tesseract; tetrahedral prism; pentatope
2010 MSC: 52B11, 65D05, 65D32, 74S05, 76M10

1. Introduction

Space-time finite element methods are a promising approach for producing highly accurate and efficient solutions to partial differential equations (PDEs). More specifically, these methods can adaptively redistribute their degrees of freedom in both space and time in order to optimally resolve critical features of the solution. Despite their potential, the application of these methods to real-world engineering problems remains an open area of research. While one may simulate space-time problems in $1d + t$ (two-dimensional space) or $2d + t$ (three-dimensional space) by leveraging well-established finite element techniques, many of these techniques do not carry over to $3d + t$ (four-dimensional space). In some sense, four-dimensional space should be approached as a new frontier, and we must recognize the unique geometric characteristics which arise in this context.

There are several specific challenges for space-time finite element methods in the areas of meshing, interpolation, and numerical integration (i.e. quadrature/cubature). In what follows, we will briefly review these challenges, along with a short discussion of the associated literature. Our focus will be limited to state-of-the-art challenges associated with polynomial-based finite element methods. Note: for a more fundamental discussion of the methods themselves, including their basic construction, one may consult the textbooks of Ern and Guermond [1], and Johnson [2], (see Chapters 6 and 8, respectively). In addition, for a discussion of non-uniform rational B-spline (NURB)-based methods, please consult the recent work on isogeometric analysis (IGA) [3, 4, 5, 6, 7, 8, 9, 10, 11].

Our first challenge is to develop unstructured space-time meshes in order to simulate problems with complex boundaries. In this setting, one may extend the traditional notion of an unstructured mesh by defining ‘fully-unstructured’ meshes as grids which are unstructured in both space and time, and ‘partially-unstructured’ meshes as grids which are unstructured in space only. The latter meshes are usually generated by extruding unstructured spatial meshes in the temporal direction. Evidently, the partially-unstructured meshes are less optimal than the fully-unstructured meshes, as all elements are required to take the same time-step. Nevertheless, fully-unstructured meshes are more difficult

to generate. The problem of mesh generation may become significantly easier if hybrid meshes are employed, however then it becomes necessary to select a suitable conforming set of elements (4-polytopes) for populating the mesh. In three-dimensional space, one may select combinations of hexahedron, triangular prism, square pyramid, and tetrahedron elements. However, in four-dimensional space there are significantly more elements to consider (as we will demonstrate). In order to avoid these complications, previous researchers have used non-hybrid meshes composed entirely by one of the following standard elements: tesseracts, tetrahedral prisms, or pentatopes. For example, partially-unstructured meshes of tesseract elements were used by van der Vegt and coworkers [12, 13, 14] along with discontinuous Galerkin (DG) methods to solve laminar compressible flow problems. In addition, Diosady and Murman [15, 16, 17, 18] have used a similar approach to solve turbulent compressible flow problems. In these studies, the primary objective has been to exploit the tensor-product structure of the tesseract and maximize computational efficiency. A contrasting approach is exemplified by Tezduyar and coworkers [19, 20, 21, 22], who used partially-unstructured meshes of tetrahedral prism elements along with Galerkin least-squares (GLS) in space/DG in time methods to solve fluid-structure interaction (FSI) problems. In these studies, the primary objective was to leverage the flexibility of unstructured tetrahedral grids for treating complicated geometries. Yang et al. [23] have used a similar approach along with a hybrid finite-difference/finite-element method to solve the *fractional* Bloch-Torrey equations for biomedical flows. (Note: for detailed discussions of fractional PDEs, including the Fredholm, Schrödinger, and shallow water equations, one may consult the writings of Al-Smadi et al. [24, 25, 26, 27], and Karniadakis and coworkers [28, 29]). In an alternative fashion, Behr [30] has shown that tetrahedral prisms can be subdivided in order to generate pentatope elements. The resulting meshes have been used by Behr and coworkers [31, 32, 33] in conjunction with GLS in space/DG in time methods to solve two-phase incompressible flow problems and single-phase compressible flow problems. In addition, Wang [34] has used these meshes in conjunction with space-time DG methods to solve compressible, viscous flow problems with rotating bodies. Furthermore, Lehrenfeld [35] has used these meshes in conjunction with enriched space-time DG methods (XFEM-DG methods) to solve convection-diffusion problems with moving bodies. These efforts (above) have all focused on partially-unstructured meshes. In order to move towards fully-unstructured meshes, Mont [36] used a tent-pitching algorithm [37] to generate unstructured pentatopic meshes that locally satisfy a causality constraint. In addition, Neumüller and Steinbach [38, 39] generated isotropic refinement strategies for fully-unstructured meshes of pentatope elements. Similar work has been subsequently performed by Foteinos et al. [40] and Belda-Ferrín et al. [41]. Most recently, Caplan and coworkers [42, 43, 44, 45] have developed highly-anisotropic, fully-unstructured meshes of pentatope elements. In principle, these meshes possess the greatest flexibility of any meshes generated to-date for discretizing space-time problems. Despite this flexibility, there are still opportunities to further improve the generality of space-time meshes by considering a broader class of elements beyond the classical tesseract, tetrahe-

dral prism, and pentatope elements; and furthermore by constructing hybrid meshes (as discussed earlier).

The next challenge is to develop a family of modal basis functions and/or nodal basis functions. For example, one may construct a modal basis on the reference tesseract $[-1, 1]^4$ by taking tensor products of one-dimensional Legendre polynomials, and a nodal basis can be constructed in a similar fashion by using Lagrange polynomials. Unfortunately, this simplicity-of-construction does not carry over to other element types. For example, the modal basis on the tetrahedral prism is usually obtained from a tensor product of the one-dimensional Legendre basis and the three-dimensional PKDO basis (originally derived in two dimensions by Proriol [46], Koornwinder [47], Dubiner [48], and Owens [49]). Once this modal basis is obtained, a nodal basis can be numerically computed using a generalized Vandermonde matrix, following the procedure on p. 410 of [50] and p. 124 of [51]. However, the resulting nodal basis functions do not have explicit expressions, and the conditioning of the Vandermonde matrix can be sensitive to the polynomial order and the placement of nodal points. In practice, the latter issue is not especially serious for low-to-moderate polynomial orders ($p \leq 6$) [50]. Note that it is possible to completely avoid this issue by explicitly constructing nodal basis functions using the Lagrange-mapping procedure of Hughes ([52] pp. 164-174). However, this procedure is not general, and must be tailored for each polynomial order. Therefore, the Vandermonde procedure of [50] is usually preferred. A similar set of issues arise for pentatope basis functions. In this case, the modal basis is chosen to be the four-dimensional PKDO basis (defined in [53]), and the nodal basis can be obtained using the aforementioned Vandermonde procedure. In summary, the construction of modal and nodal basis functions for tesseract, tetrahedral prism, and pentatope elements is well-established, with some caution required for nodal basis functions at high polynomial orders. Nevertheless, there does not appear to be a well-known resource which aggregates these basis function definitions in one place. In addition, there does not appear to be any research on the construction of modal or nodal basis functions for non-standard element types.

The last challenge is to numerically integrate polynomial functions and transcendental functions on each element. One can easily construct quadrature rules for the standard tesseract element by taking tensor products of one-dimensional Gauss-Legendre rules. The resulting rules are ‘good’ in the following sense: i) they exactly integrate polynomials of degree $\leq p$, where $p = 2M - 1$ and M is the number of quadrature points in one dimension; ii) all quadrature points reside strictly within the tesseract; iii) all quadrature points are arranged symmetrically; and iv) all quadrature weights are positive. Unfortunately, while tensor-product rules are ‘good’, they are not optimal as they possess an excessive number of quadrature points ($N_p = M^4$ points). Furthermore, they cannot be mapped to tetrahedral prism or pentatope elements without violating symmetry. As a result, it is important to generate good, non-tensor-product rules which are optimized for each element type. In what follows, we briefly review the best known quadrature rules of this kind on the tesseract and pentatope. Note: to the authors’ knowledge, no such rules have been constructed for the

tetrahedral prism. On the tesseract, Stroud [54], and Sørøvik and Espelid [55] constructed rules which exactly integrate polynomials of degrees $p = 3$ and 5, with 8 and 24 points, respectively. Thereafter, Majorana et al. [56], and Sørøvik and Espelid [57] constructed a rule which exactly integrates a polynomial of degree $p = 7$ with 57 points. Finally, Sørøvik [58] discovered a rule which exactly integrates a polynomial of degree $p = 9$ with 160 points. In a similar fashion, many researchers have constructed quadrature rules for the pentatope (see the recent review in [59]). In particular, Hammer and Stroud [60, 61] constructed rules which exactly integrate polynomials of degrees $p = 2$ and 3, with 5 and 15 points, respectively (although the latter rule has points on the boundary). Thereafter, Gusev et al. [62] have constructed rules which exactly integrate polynomials of degrees 4, 5, 6, 7, and 8 with 20, 30, 56, 76, and 110 points, respectively. In summary, there is a critical absence of good quadrature rules capable of exactly integrating polynomials with $p \gtrsim 9$ on tesseract and pentatope elements. Furthermore, only tensor-product based rules are known to exist on the tetrahedral prism.

The purpose of this article is to address some of the key shortcomings discussed above. In particular, we will: i) identify new types of space-time elements, and ii) review/expand the interpolation and integration procedures associated with tesseract, tetrahedral prism, and pentatope elements. The format of this article is as follows. In section 2, we describe a systematic procedure for generating sequences of space-time elements. In section 3, we define the standard tesseract, tetrahedral prism, and pentatope reference elements, and review their essential properties, including their symmetry groups and orthonormal basis functions. In section 4, we describe a computational strategy for constructing quadrature rules on these standard elements. Thereafter, in sections 5 and 6, we summarize the resulting quadrature rules, and demonstrate their effectiveness on a suite of numerical experiments. Finally, in section 7, we summarize the main conclusions of the article.

2. Identification of Element Sequences

In this section, our objective is to construct sequences of space-time elements. Evidently, there are an infinite number of possible sequences, and within each sequence there are an unlimited number of polytopes which can be considered. However, for the sake of convenience, we narrow our focus to finite sequences of convex polytopes which can be formed by degenerating the vertices of the tesseract. These polytopes are most amenable to practical applications, as in principle, a polynomial basis can be formed on each element by constructing a suitable mapping from the tesseract to the associated subpolytope. In what follows, we will generate sequences of elements in this fashion, and introduce formal mathematical notation and terminology to aid in this process.

The unit d -cube (d -dimensional cube) is the d -polytope I^d , the d -fold prism of the unit interval $I = [0, 1]$. Its vertices are all points of the form (x_1, \dots, x_d) such that each x_i equals either 0 or 1. A 0/1-polytope P is the convex hull of a nonempty subset V of the vertices of the d -cube; in other words, the vertex

set of P , $\text{vert}(P)$, will be denoted by V . If V consists of the points $(0, \dots, 0)$, $(1, 0, \dots, 0)$, $(0, 1, 0, \dots, 0)$, \dots , $(0, 0, \dots, 0, 1)$, we will call P the standard d -simplex. See [63, 64, 65, 66] for a description of some of the properties of 0/1-polytopes.

In the remainder of this section, we describe the construction of two sequences of d -elements (d -dimensional elements). These sequences are noteworthy, as for $d = 2$ and $d = 3$ they contain standard elements which are frequently used to construct 2D and 3D meshes. Naturally, here we are interested in the generalization of these sequences to 4D, and possibly higher dimensions.

First, let us consider the construction of the following sequence

$$P_0, P_1, \dots, P_{2^d-2d}, \dots, P_{2^d-d-1}$$

together with a sequence of 0/1-points

$$v_0, \dots, v_{2^d-d-2}$$

with the following properties:

- The element P_i is a d -dimensional 0/1-polytope, $i = 0, \dots, 2^d - d - 1$.
- The point v_i is a vertex of P_i , $i = 0, \dots, 2^d - d - 2$.
- The element P_{i+1} is the convex hull of $\text{vert}(P_i) \setminus v_i$, $i = 0, \dots, 2^d - d - 2$. Thus P_{i+1} is the result of degenerating the vertex v_i of P_i .
- The first element of the sequence P_0 is the unit d -cube.
- The intermediate element of the sequence P_{2^d-2d} is a prism formed by extruding the $(d-1)$ -simplex into one dimension higher. In other words, the element P_{2^d-2d} is a prism over the standard $(d-1)$ -simplex.
- The last element of the sequence P_{2^d-d-1} is the standard d -simplex.

Note in particular that when $d = 4$, then the 3-simplex is a 3-dimensional tetrahedron, and P_8 is the tetrahedral prism obtained by extruding the tetrahedron in the direction of the fourth coordinate.

The construction of the sequence is recursive on $d = 1, 2, \dots$. Naturally, when $d = 1$, $P_0 = P_{2^d-2d} = P_{2^d-d-1} = [0, 1]$ and the vertex sequence is empty. When $d = 2$, $v_0 = (1, 1)$, $P_0 = P_{2^d-2d}$ (the unit square), and $P_1 = P_{2^d-d-1}$ (the standard 2-simplex). For $d \geq 3$, the vertex sequence v'_i in dimension d is constructed from the vertex sequence $v_0, \dots, v_{2^{d-1}-(d-1)-2}$ in dimension $d-1$ by using the following steps.

1. For each vertex v_i create two new vertices $v'_{2i} = (v_i, 1)$ and $v'_{2i+1} = (v_i, 0)$ by appending to v_i first a 1 and second a 0, for $i = 0, \dots, 2^{d-1} - (d-1) - 2$. The result is $v'_0, \dots, v'_{2^d-2d-1}$.
2. Complete the sequence by setting $v'_{2^d-2d} = (1, 0, 0, 0, \dots, 0, 1)$, $v'_{2^d-2d+1} = (0, 1, 0, 0, \dots, 0, 1)$, $v'_{2^d-2d+2} = (0, 0, 1, 0, \dots, 0, 1)$, $\dots, v'_{2^d-d-2} = (0, 0, 0, 0, \dots, 1, 1)$.

If we regard the d -cube as a prism over the $(d - 1)$ -cube, the above sequence of degenerations alternates by removing a vertex of the ‘upper’ $(d - 1)$ -cube, followed by removing the corresponding vertex of the ‘lower’ $(d - 1)$ -cube, thus replicating the $(d - 1)$ -dimensional degeneration sequence on both the top and the bottom. At the end of phase 1 above, we will have a prism over the standard $(d - 1)$ -simplex. (In fact, P'_{2^i} will be a prism over P_i , $i = 0, \dots, 2^{d-1} - d - 1$.) From that point on, the sequence in phase 2 strips away vertices on the top until a single point remains, resulting in a standard d -simplex.

Table 1 shows the vertex sequences for dimensions 2, 3, and 4. (For convenience we use an abbreviated form of the vertex coordinates.)

$d = 2$	$d = 3$	$d = 4$
11	111	1111
	110	1110
	101	1101
	011	1100
		1011
		1010
		0111
		0110
		1001
		0101
		0011

Table 1: Sequences of vertices in low dimensions

For $d = 3$ the resulting elements P_i are displayed in Figure 1.

For $d = 4$ the resulting elements P'_i are displayed in Figure 2. Here, the depictions are Schlegel diagrams—central projections of 4-polytopes onto a 3-dimensional hyperplane with respect to a point placed close to a facet (3-face) of the 4-polytope; see [67]. In particular, P'_0 is the tesseract (4-cube), P'_8 is a tetrahedral prism (prism over the standard 3-simplex), and P'_{11} is the pentatope (4-simplex). Note that P'_0, P'_2, P'_4, P'_6 are prisms over, respectively, the 3-dimensional elements P_0, P_1, P_2, P_3 of Figure 1.

The second vertex sequence of interest is the one obtained by regarding the vertices of the d -cube as numbers expressed in binary notation. One may list them in decreasing order, but omit the vertices of the standard d -simplex. The corresponding low dimensional sequences are shown in Table 2. When $d = 3$ this sequence matches the earlier one, but they are different when $d \geq 4$. In particular, this sequence does not contain the tetrahedral prism. For $d = 4$ the resulting elements P'_i are displayed in Figure 3.

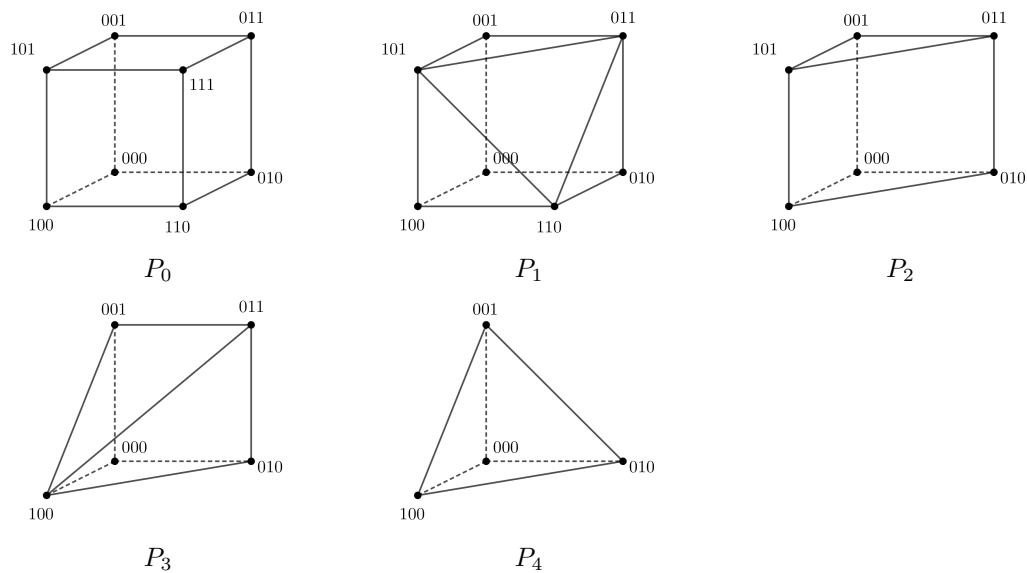


Figure 1: Sequence of elements in dimension 3

$d = 2$	$d = 3$	$d = 4$
11	111	1111
	110	1110
	101	1101
	011	1100
		1011
		1010
		1001
		0111
		0110
		0101
		0011

Table 2: Decreasing binary sequences of vertices in low dimensions

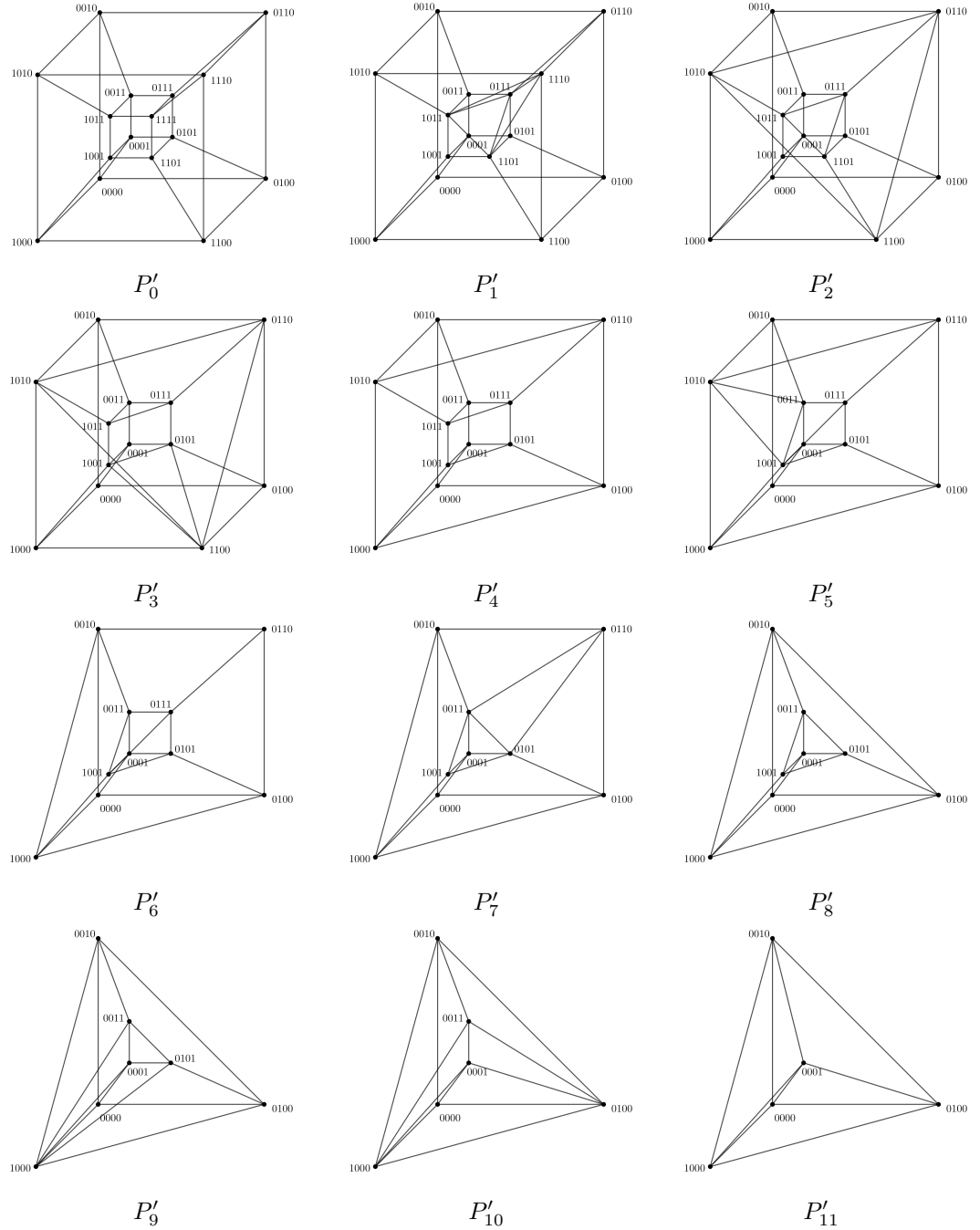


Figure 2: Sequence of elements in dimension 4

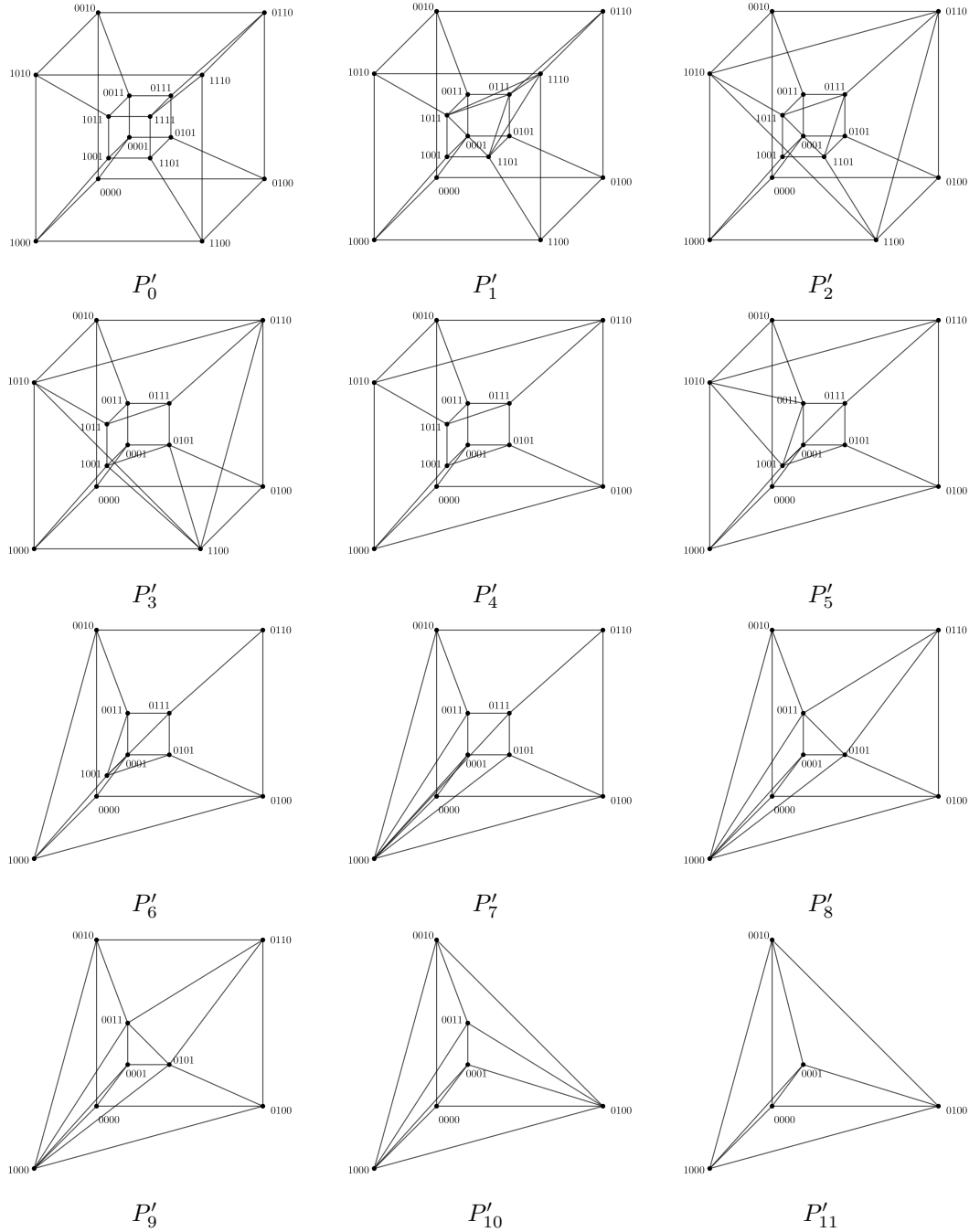


Figure 3: Second sequence of elements in dimension 4

These two types of sequences are far from exhaustive, since the number of combinatorially inequivalent 0/1 d -polytopes increases doubly-exponentially with d —see [63]. For example, for $d = 4$ there are 60,879 such 0/1 d -polytopes [68]. Nevertheless, we have highlighted the two sequences above because for $d = 2$ and $d = 3$ they contain elements which are frequently used in conventional finite element methods (as we mentioned previously). Furthermore, for $d = 4$ they contain new element types. Finally, the first sequence also contains all of the standard 4D element types such as the tesseract, the tetrahedral prism, and the pentatope. In the next few sections, we will focus on developing numerical interpolation and integration procedures for these standard 4D elements.

3. Polynomial Bases and Symmetry Groups

3.1 Overview

In the previous section, we constructed sequences of elements based on degenerations of the 4-cube $[0, 1]^4$, and we recovered the standard tesseract, tetrahedral prism, and pentatope elements. Our choice of the interval $[0, 1]$ was consistent with standard mathematical conventions, however, for engineering purposes it is common practice to use the interval $[-1, 1]$ instead. For certain operations (such as interpolation and integration) this interval is more convenient, as it is symmetrical and centered at the origin. Of course, formally speaking, the mathematical and engineering intervals are topologically equivalent, as they are related by a linear map. Therefore, the intervals are interchangeable, and we have a free choice of which one to use.

In what follows, we switch to the engineering convention, and construct a new set of reference elements for the tesseract, tetrahedral prism, and pentatope. In addition, we discuss the essential properties of these elements which are useful for implementation purposes. In particular, integration bounds are introduced in order to define the domains of our reference elements, basis functions on each reference element are constructed for interpolation and quadrature purposes, and lastly we define symmetry groups for each reference element in order to facilitate the generation of fully symmetric quadrature rules.

3.2 Preliminaries

Throughout this section, whenever we develop basis functions, we construct an orthonormal basis, i.e.,

$$\int_{\Omega} \psi_{ijkq}(\mathbf{x}) \psi_{rstv}(\mathbf{x}) d\mathbf{x} = \delta_{ir} \delta_{js} \delta_{kt} \delta_{qv},$$

where δ_{ir} is the Kronecker delta. The simplest orthonormal basis functions of degree p have the form

$$\psi_{ijkq}(\mathbf{x}) = \zeta_{ijkq} \hat{P}_i^{(\alpha_1, \beta_1)}(a) \hat{P}_j^{(\alpha_2, \beta_2)}(b) \hat{P}_k^{(\alpha_3, \beta_3)}(c) \hat{P}_q^{(\alpha_4, \beta_4)}(d),$$

where $0 \leq i + j + k + q \leq p$, $a = a(x_1, x_4)$, $b = b(x_2, x_4)$, $c = c(x_3, x_4)$, and $d = d(x_4)$ are functions depending on the element type, ζ_{ijkq} , $\alpha_1, \dots, \alpha_4$ and

β_1, \dots, β_4 are constants, and $\hat{P}_n^{(\alpha, \beta)}$ is the 1D orthonormal Jacobi polynomial defined as

$$\hat{P}_n^{(\alpha, \beta)}(x) = \frac{P_n^{(\alpha, \beta)}(x)}{\sqrt{\frac{2^{\alpha+\beta+1}}{2n+\alpha+\beta+1} \frac{(n+\alpha)!(n+\beta)!}{n!(n+\alpha+\beta)!}}}.$$

Here, $P_n^{(\alpha, \beta)}$ is the standard orthogonal (but not orthonormal) Jacobi polynomial.

3.3 Tesseract

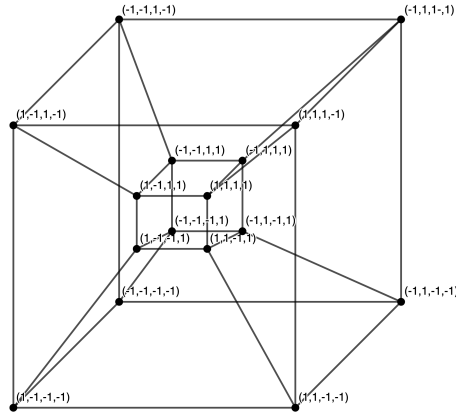


Figure 4: Tesseract reference element.

The first reference element is the tesseract with edge length 2 and volume 16 shown in Figure 4. It is straightforward to define bounds of integration as follows

$$\int_{-1}^1 \int_{-1}^1 \int_{-1}^1 \int_{-1}^1 dx_1 dx_2 dx_3 dx_4 = 16.$$

Trivially, the orthonormal basis inside of the reference tesseract is given by

$$\psi_{ijkq}(\mathbf{x}) = \hat{P}_i(a) \hat{P}_j(b) \hat{P}_k(c) \hat{P}_q(d),$$

where $0 \leq i, j, k, q \leq p$, $a = x_1$, $b = x_2$, $c = x_3$, and $d = x_4$. There are a total of $N_{\text{dof}} = (p+1)^4$ basis functions.

The tesseract has a total of 384 symmetries. We can apply these symmetries to a point $(\alpha, \beta, \gamma, \delta)$ with the constraints $0 \leq \alpha, \beta, \gamma, \delta \leq 1$. This will yield a set $\chi(\alpha, \beta, \gamma, \delta)$ containing its counterparts noting that χ denotes the permutations. The cardinality of χ depends on if any of the symmetries give rise to identical points. By enumerating this process with the conditions above we obtain twelve

symmetry orbits (groups)

$S_1 = (0, 0, 0, 0),$	$ S_1 = 1,$
$S_2(\alpha) = \chi(\alpha, 0, 0, 0),$	$ S_2 = 8,$
$S_3(\alpha) = \chi(\alpha, \alpha, 0, 0),$	$ S_3 = 24,$
$S_4(\alpha, \beta) = \chi(\alpha, \beta, 0, 0),$	$ S_4 = 48,$
$S_5(\alpha) = \chi(\alpha, \alpha, \alpha, 0),$	$ S_5 = 32,$
$S_6(\alpha, \beta) = \chi(\alpha, \alpha, \beta, 0),$	$ S_6 = 96,$
$S_7(\alpha, \beta, \gamma) = \chi(\alpha, \beta, \gamma, 0),$	$ S_7 = 192,$
$S_8(\alpha) = \chi(\alpha, \alpha, \alpha, \alpha),$	$ S_8 = 16,$
$S_9(\alpha, \beta) = \chi(\alpha, \alpha, \alpha, \beta),$	$ S_9 = 64,$
$S_{10}(\alpha, \beta) = \chi(\alpha, \alpha, \beta, \beta),$	$ S_{10} = 96,$
$S_{11}(\alpha, \beta, \gamma) = \chi(\alpha, \alpha, \beta, \gamma),$	$ S_{11} = 192,$
$S_{12}(\alpha, \beta, \gamma, \delta) = \chi(\alpha, \beta, \gamma, \delta),$	$ S_{12} = 384.$

3.4 Tetrahedral Prism

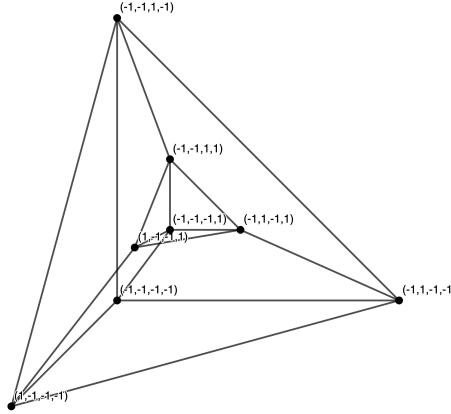


Figure 5: Tetrahedral prism reference element.

Our second reference element is the tetrahedral prism which is created by an extrusion of a standard tetrahedron into four dimensional space; the element itself is shown in Figure 5. (Note: the standard tetrahedron is the three dimensional extension of the right triangle.) The volume of the tetrahedral prism is $\frac{8}{3}$. The integration bounds for the tetrahedral prism are similar to the standard tetrahedron while accounting for the extrusion in the fourth dimension,

$$\int_{-1}^1 \int_{-1}^1 \int_{-1}^{-x_3} \int_{-1}^{-1-x_2-x_3} dx_1 dx_2 dx_3 dx_4 = \frac{8}{3}.$$

Furthermore, the orthonormal polynomial basis for the tetrahedral prism is found by extending the tetrahedron basis in [53, 50, 69],

$$\psi_{ijkq}(\mathbf{x}) = \sqrt{8} \hat{P}_i(a) \hat{P}_j^{(2i+1,0)}(b) \hat{P}_k^{(2i+2j+2,0)}(c) \hat{P}_q(d) (1-b)^i (1-c)^{i+j},$$

where $0 \leq i + j + k \leq p$, $0 \leq q \leq p$, $a = -2 \frac{1+x_1}{x_2+x_3} - 1$, $b = 2 \frac{1+x_2}{1-x_3} - 1$, $c = x_3$, $d = x_4$, and $N_{\text{dof}} = (p+1)^2 (p+2) (p+3) / 6$.

For this element, it is convenient to work in barycentric coordinates due to the two tetrahedral facets. The barycentric coordinates are specified as follows

$$\boldsymbol{\lambda} = (\lambda_1, \lambda_2, \lambda_3, \lambda_4, x_4)^T \quad \text{where } 0 \leq \lambda_i \leq 1, \quad \lambda_1 + \lambda_2 + \lambda_3 + \lambda_4 = 1.$$

They are related to Cartesian coordinates by

$$\mathbf{x} = \begin{pmatrix} -1 & 1 & -1 & -1 & 0 \\ -1 & -1 & 1 & -1 & 0 \\ -1 & -1 & -1 & 1 & 0 \\ 0 & 0 & 0 & 0 & 1 \end{pmatrix} \boldsymbol{\lambda}.$$

The symmetry orbits of the tetrahedral prism are similar to those of the tetrahedron, with an additional parameter that accounts for the extension of the prism in the fourth dimension. There are 48 total symmetries for the tetrahedral prism, and the symmetry orbits are written as follows

$$\begin{aligned} S_1 &= \left(\frac{1}{4}, \frac{1}{4}, \frac{1}{4}, \frac{1}{4}, 0\right), & |S_1| &= 1, \\ S_2(\delta) &= \left(\frac{1}{4}, \frac{1}{4}, \frac{1}{4}, \frac{1}{4}, \pm\delta\right), & |S_2| &= 2, \\ S_3(\alpha) &= \chi(\alpha, \alpha, \alpha, 1 - 3\alpha, 0), & |S_3| &= 4, \\ S_4(\alpha, \delta) &= \chi(\alpha, \alpha, \alpha, 1 - 3\alpha, \pm\delta), & |S_4| &= 8, \\ S_5(\alpha) &= \chi(\alpha, \alpha, \frac{1}{2} - \alpha, \frac{1}{2} - \alpha, 0), & |S_5| &= 6, \\ S_6(\alpha, \delta) &= \chi(\alpha, \alpha, \frac{1}{2} - \alpha, \frac{1}{2} - \alpha, \pm\delta), & |S_6| &= 12, \\ S_7(\alpha, \beta) &= \chi(\alpha, \alpha, \beta, 1 - 2\alpha - \beta, 0), & |S_7| &= 12, \\ S_8(\alpha, \beta, \delta) &= \chi(\alpha, \alpha, \beta, 1 - 2\alpha - \beta, \pm\delta), & |S_8| &= 24, \\ S_9(\alpha, \beta, \gamma) &= \chi(\alpha, \beta, \gamma, 1 - \alpha - \beta - \gamma, 0), & |S_9| &= 24, \\ S_{10}(\alpha, \beta, \gamma, \delta) &= \chi(\alpha, \beta, \gamma, 1 - \alpha - \beta - \gamma, \pm\delta), & |S_{10}| &= 48, \end{aligned}$$

where α , β , and γ are constrained to ensure that $0 \leq \lambda_i \leq 1$, $\sum_i \lambda_i = 1$ and $0 \leq \delta \leq 1$.

3.5 Pentatope

The final reference element shown in Figure 6 is the pentatope or standard four-dimensional simplex which has a volume of $\frac{2}{3}$. The bounds of integration are

$$\int_{-1}^1 \int_{-1}^{-x_4} \int_{-1}^{-1-x_3-x_4} \int_{-1}^{-2-x_2-x_3-x_4} dx_1 dx_2 dx_3 dx_4 = \frac{2}{3}.$$

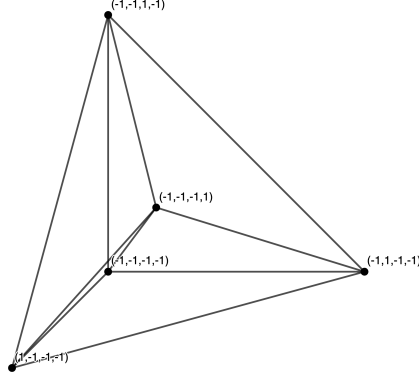


Figure 6: Pentatope reference element.

The orthonormal polynomial basis for the pentatope is obtained from the generalized simplex formula presented in [53]

$$\begin{aligned} \psi_{ijkq}(\mathbf{x}) &= 4\hat{P}_i(a) \hat{P}_j^{(2i+1,0)}(b) \hat{P}_k^{(2i+2j+2,0)}(c) \hat{P}_q^{(2i+2j+2k+3,0)}(d) \\ &\quad \times (1-b)^i (1-c)^{i+j} (1-d)^{i+j+k}, \end{aligned}$$

where $0 \leq i + j + k + q \leq p$, $a = -2\frac{x_1+1}{x_2+x_3+x_4+1} - 1$, $b = -2\frac{1+x_2}{x_3+x_4} - 1$, $c = 2\frac{1+x_3}{1-x_4} - 1$, $d = x_4$, and $N_{\text{dof}} = (p+1)(p+2)(p+3)(p+4)/24$. Similar to the tetrahedron, it is convenient to work in barycentric coordinates. For the pentatope these are

$$\boldsymbol{\lambda} = (\lambda_1, \lambda_2, \lambda_3, \lambda_4, \lambda_5)^T \quad \text{where } 0 \leq \lambda_i \leq 1, \quad \lambda_1 + \lambda_2 + \lambda_3 + \lambda_4 + \lambda_5 = 1,$$

and are related to Cartesian coordinates by

$$\mathbf{x} = \begin{pmatrix} -1 & 1 & -1 & -1 & -1 \\ -1 & -1 & 1 & -1 & -1 \\ -1 & -1 & -1 & 1 & -1 \\ -1 & -1 & -1 & -1 & 1 \end{pmatrix} \boldsymbol{\lambda}.$$

Note that the columns of the matrix correspond to the vertices of the pentatope in Cartesian coordinates. The pentatope has a total of 120 symmetries as shown in [70], which take the following form

$$\begin{aligned} S_1 &= \left(\frac{1}{5}, \frac{1}{5}, \frac{1}{5}, \frac{1}{5}, \frac{1}{5}\right), & |S_1| &= 1, \\ S_2(\alpha) &= \chi(\alpha, \alpha, \alpha, \alpha, 1 - 4\alpha), & |S_2| &= 5, \\ S_3(\alpha) &= \chi\left(\alpha, \alpha, \alpha, \frac{1}{2} - \frac{3}{2}\alpha, \frac{1}{2} - \frac{3}{2}\alpha\right), & |S_3| &= 10, \\ S_4(\alpha, \beta) &= \chi(\alpha, \alpha, \alpha, \beta, 1 - 3\alpha - \beta), & |S_4| &= 20, \\ S_5(\alpha, \beta) &= \chi(\alpha, \alpha, \beta, \beta, 1 - 2\alpha - 2\beta), & |S_5| &= 30, \\ S_6(\alpha, \beta, \gamma) &= \chi(\alpha, \alpha, \beta, \gamma, 1 - 2\alpha - \beta - \gamma), & |S_6| &= 60, \\ S_7(\alpha, \beta, \gamma, \delta) &= \chi(\alpha, \beta, \gamma, \delta, 1 - \alpha - \beta - \gamma - \delta), & |S_7| &= 120, \end{aligned}$$

where α , β , γ , and δ are constrained to ensure that $0 \leq \lambda_i \leq 1$, $\sum_i \lambda_i = 1$.

4. Solution Strategy for Quadrature Rules

4.1 Our approach

In this section, we describe a strategy for generating symmetric quadrature rules on space-time elements. Note that this strategy leverages the numerical infrastructure which was developed in the previous section.

The task of identifying a quadrature rule of strength \mathcal{P} inside of a domain Ω can be framed as a non-linear optimization problem where we seek a set of N_p abscissa $\{\mathbf{x}_i\}$ and associated weights $\{\omega_i\}$ such that

$$\int_{\Omega} g_{rstv}(\mathbf{x}) d\mathbf{x} = \sum_{i=1}^{N_p} \omega_i g_{rstv}(\mathbf{x}_i) \quad \text{for} \quad 0 \leq r + s + t + v \leq \mathcal{P}, \quad (4.1)$$

where $g_{rstv}(\mathbf{x}) = x_1^r x_2^s x_3^t x_4^v$ and $r, s, t, v \geq 0$. When we evaluate the left hand side of this equation, the resulting system is a *non-linear least squares problem*; albeit one where we seek a solution whose residual is zero. Moreover, as formulated in Eq. (4.1), the system is ill-conditioned and fails to enforce the requirements that the resulting rules are symmetric, have positive weights, and have points which are contained within the domain of integration.

The first issue involving ill-conditioning can be addressed by taking

$$g_{rstv}(\mathbf{x}) = \psi_{rstv}(\mathbf{x}),$$

where $\psi_{rstv}(\mathbf{x})$ corresponds to the orthonormal polynomial basis for Ω as defined in Section 3. Moreover, on account of the orthogonality of the basis, it follows that

$$\int_{\Omega} \psi_{rstv}(\mathbf{x}) d\mathbf{x} = c \delta_{0r} \delta_{0s} \delta_{0t} \delta_{0v},$$

where $c = 1/\psi_{0000}$. This enables us to forego having to directly evaluate integrals inside of our domain in order to formulate our non-linear least squares problem.

The second issue involving symmetry can be resolved by decomposing the N_p points into a set of symmetry groups (orbits). For example, consider taking Ω to be the pentatope and N_p to be 61. One possible symmetric arrangement of these points involves a combination of an S_1 orbit, an S_3 orbit, an S_4 orbit, and an S_5 orbit. Summing the number of points generated by each orbit we find

$$1 + 10 + 20 + 30 = 61,$$

as required. By symmetry, it clearly must be the case that all points belonging to an orbit must share the same quadrature weight. Noting that an S_1 orbit has no parameters, S_3 orbits have one parameter, and S_4 and S_5 orbits both have two parameters, our non-linear least squares problem has a total of 9 parameters; 5 from the orbits and 4 from the associated quadrature weights. This is a

substantial reduction compared to the $61 \times 4 + 61 = 305$ parameters in our original—*asymmetric*—problem. This greatly reduces the difficulty associated with obtaining an exact solution to the non-linear least squares problem. The caveat here is that, in general, we do not know precisely which of the many distinct orbital decompositions is the correct one. For example, in the case where $N_p = 61$ in a pentatope, there are 24 unique decompositions, including the one we’ve already presented. Others include a decomposition with one S_1 orbit, four S_2 orbits, one S_3 orbit, and an S_5 orbit for a total of 61 points defined by 14 parameters, and another decomposition with one S_1 orbit and 12 S_2 orbits for a total of 61 points defined by 25 parameters. Given that there is no *a priori* means of ascertaining which orbit is most likely to yield a rule, it is generally necessary to try *all* of these decompositions. Moreover, we remark here that the number of decompositions grows rapidly with N_p . When $N_p = 600$ there are some 37,457 decompositions inside of the pentatope.

Symmetry also enables us to reduce the number of basis functions which must be included in our non-linear least squares problem. Specifically, the ability of a rule to exactly integrate one particular basis function oftentimes implies that it is also capable of exactly integrating other basis functions, too. For example, inside of a tesseract, if a rule is capable of integrating $\psi_{rstv}(\mathbf{x})$ then, by symmetry, it must also be able to integrate $\psi_{srtv}(\mathbf{x})$ and all other permutations thereof. This enables us to substantially reduce the size of the non-linear least squares problem.

The third issue involving positivity of the quadrature weights can be addressed in a variety of ways. One possibility is to compute them using a *non-negative least squares* routine. However, the performance of such routines is typically not competitive with those of ordinary linear least squares solvers. As such, we have found it more efficient to introduce a penalty parameter to the non-linear least squares problem. Specifically, we add an additional equation into the non-linear system which vanishes if all the weights are positive

$$\varepsilon = \sum_{i=1}^{N_p} \frac{\omega_i - |\omega_i|}{2}.$$

The fourth issue involving confinement of quadrature points to Ω can also be addressed in a variety of ways. One is to employ a non-linear least squares solver with support for linear equality constraints. However, such solvers are less widespread than unconstrained non-linear least squares solvers. An alternative approach (used here), which foregoes the need for explicit constraints, is to simply *clamp* or cut off the relevant orbital parameters before passing them to the S_i orbital functions which yield the Cartesian points. This clamping discourages the solver from attempting to take orbital parameters outside of their respective ranges.

Another final improvement we can make to our baseline algorithm is to observe that the non-linear least squares problem is *separable*. If the orbital parameters—which define the abscissa—are known then our non-linear least squares problem in Eq. (4.1) reduces down to a *linear* least squares problem

for the ω_i . Thus, it is possible to treat the quadrature weights as *dependent* variables. This enables us to further reduce the size of the non-linear least squares problem; albeit at the cost of having to solve a linear least squares problem at each iteration.

4.2 Alternative approaches

We remark here that in the case of the tesseract that it is possible to generate symmetric rules through a tensor-product construction of a suitable one-dimensional rule. If a Gauss–Legendre rule with $l + 1$ points is employed, it follows that the resulting tesseract rule has $(l + 1)^4$ points and is capable of exactly integrating $g_{rstv}(\mathbf{x})$ for $0 \leq r, s, t, v \leq 2l + 1$. This property leads to the rules being extremely efficient for integrating functions with a tensor-product structure. Moreover, when paired with sum-factorization they can enable computationally efficient spectral element discretizations [71].

It is also possible to apply these tensor product rules to tetrahedral prisms and pentatopes by employing the well-known Duffy transformation [72]. In what follows, we briefly review the Duffy-based procedure for generating quadrature rules on the pentatope. One is encouraged to consult the appendix of [35] for more details about the origins of the Duffy transformation.

We begin by introducing $\mathbf{y} = (y_1, y_2, y_3) \in \mathbb{R}^3$ and $\mathbf{x} = (\mathbf{y}, t) \in \mathbb{R}^4$. Next, we construct the following linear map

$$(\mathbf{y}, t) \rightarrow \left(\frac{2\mathbf{y} + (1+t)\mathbf{1}}{1-t}, t \right) = (\mathbf{y}', t),$$

where $\mathbf{1} = (1, 1, 1)$. Thereafter, this map can be used to reformulate a generic integral on the reference pentatope as follows

$$\begin{aligned} & \int_{-1}^1 \int_{-1}^{-t} \int_{-1}^{-1-t-y_3} \int_{-1}^{-2-t-y_3-y_2} f(\mathbf{y}, t) dy_1 dy_2 dy_3 dt \\ &= \frac{1}{8} \int_{-1}^1 (1-t)^3 \int_{-1}^1 \int_{-1}^{-y'_3} \int_{-1}^{-1-y'_3-y'_2} f\left(\frac{(1-t)\mathbf{y}' - (1+t)\mathbf{1}}{2}, t\right) dy'_1 dy'_2 dy'_3 dt \\ &= \frac{1}{8} \int_{-1}^1 (1-t)^3 \int_{-1}^1 \int_{-1}^{-y'_3} \int_{-1}^{-1-y'_3-y'_2} g(\mathbf{y}', t) d\mathbf{y}' dt \\ &= \frac{1}{8} \int_{-1}^1 (1-t)^3 G(t) dt, \end{aligned} \tag{4.2}$$

where on the last two lines we have introduced the following quantities

$$\begin{aligned} g(\mathbf{y}', t) &= f\left(\frac{(1-t)\mathbf{y}' - (1+t)\mathbf{1}}{2}, t\right), \\ G(t) &= \int_{-1}^1 \int_{-1}^{-y'_3} \int_{-1}^{-1-y'_3-y'_2} g(\mathbf{y}', t) d\mathbf{y}'. \end{aligned} \tag{4.3}$$

The key observation is that the integral in Eq. (4.3) is a three-dimensional integral over the standard tetrahedron. Therefore, one may utilize a generic three-dimensional integration formula to evaluate Eq. (4.3), in conjunction with a 1D Gauss-Legendre rule for evaluating Eq. (4.2). In this fashion, the Duffy transformation replaces a four-dimensional integration procedure with a combination of three- and one-dimensional procedures. Furthermore, the transformation can be repeated recursively until only 1D Gauss-Legendre rules are required. In this case, the Duffy transformation effectively maps a Gauss-Legendre tensor-product rule from the standard tesseract on to the standard pentatope.

Somewhat unsurprisingly, none of the rules which arise from the Duffy transformation are optimal. In addition, although such rules are functional and easy to generalize, they are asymmetric and suffer from an undesirable clustering of points.

5. Summary of Quadrature Rules

Using the optimisation procedure outlined in Section 4, we obtained a series of symmetric quadrature rules on the tesseract, tetrahedral prism, and pentatope. The implementation was carried out by modifying the polyquad code, an open-source, parallel, highly robust quadrature-generating code written in C++ (see [69] for details). The resulting quadrature rules, which span orders 2 to 16, are summarised in Table 3. In addition, Table 4 contains an example of a new rule with strength $\mathcal{P} = 9$ and number of points $N_p = 151$ on the pentatope. All of the rules—**which are provided as electronic supplementary material**—have positive weights with none of the points being outside of the domain. Looking at Table 3, there are several points of note. Firstly, due to symmetry all of the tesseract rules are capable of exactly integrating *any* odd function—including odd-degree polynomials. A consequence of this is that all of the even rules pick up an extra order of accuracy. Secondly, we also note that the rules in the tetrahedral prism are limited to $\mathcal{P} = 14$, whereas those inside of the tesseract and the pentatope go up to $\mathcal{P} = 16$. This is due to the fact that the number of unique topological arrangements of points is an order of magnitude higher in the tetrahedral prism than in the other elements. As such, it is necessary to consider a greater number of non-linear least squares problems, which in turn, translates into an increased computational cost.

\mathcal{P}	N_p		
	Tesseract	Pentatope	Tetrahedral prism
2	16	5	<u>6</u>
3	16	15	<u>12</u>
4	24	20	<u>20</u>
5	24	30	<u>27</u>
6	57	56	<u>61</u>
7	57	<u>70</u>	<u>72</u>
8	160	<u>105</u>	<u>114</u>
9	160	<u>151</u>	<u>159</u>
10	<u>272</u>	<u>210</u>	<u>259</u>
11	<u>272</u>	<u>281</u>	<u>322</u>
12	<u>512</u>	<u>445</u>	<u>468</u>
13	<u>512</u>	<u>555</u>	<u>608</u>
14	<u>728</u>	<u>725</u>	<u>921</u>
15	<u>728</u>	<u>905</u>	
16	<u>1384</u>	<u>1055</u>	

Table 3: Number of points N_p required for a rule of strength \mathcal{P} inside of each element type. Note that each newly discovered quadrature rule has been underlined. In addition, the explicit parameters (weights and abscissa) for each rule are provided in the electronic supplemental material, in quadruple precision.

Orbit	Abscissa	Weight
S_1	0.20000000000000000000000000000000	0.026283450664919790544554931007647
S_2	0.033396077194956640848502386475095	0.00095166545512843622669550284918655
S_2	0.24389669924344346067467117680514	0.010657347396678176509183437341993
S_3	0.0050791921061062008978905902787788	0.00031411345650965132958719133177732
S_3	0.2967495659603128481315951580135	0.011334029741446587013061345750027
S_4	0.039703540947493234138821823418935 0.18556651270749874050254409289523	0.0034567258020126958766999595741076
S_4	0.098399070565063719667340340181978 0.25309277814594493439811072010579	0.0089501016561121758766577213589523
S_4	0.15177815296591115799210754308869 0.011737624799814566830560054028264	0.0042400257059868015877992812892785
S_5	0.0088561456625601727465721736167059 0.21639650331182284793855392295174	0.0015526370637512027432010914510579
S_5	0.085781201932866919896943973150337 0.41353118973888920995638429357091	0.0028780181522793959965686558635525

Table 4: The $\mathcal{P} = 9$ quadrature rule on the pentatope with $N_p = 151$ points. The remaining rules are provided in the electronic supplemental material, in quadruple precision.

6. Numerical Experiments

In order to validate the quadrature rules developed in Section 5, we will now perform a set of numerical experiments on the rules of strength 6-12. First, we will validate that the quadrature rules of degree \mathcal{P} exactly integrate polynomials of total order $p \leq \mathcal{P}$, to within machine precision. Thereafter, we will evaluate the ability of the quadrature rules to integrate transcendental functions reliably, with well-behaved approximation capabilities. All experiments in the following section are performed using quad-precision numerical computations to avoid precision issues.

6.1 Integration of polynomial functions on solitary elements

Let us consider the integration of polynomials of total order p , which can be given by

$$f_{\text{poly}}(\mathbf{x}; p) = \sum_{\substack{r+s+t+v \leq p \\ (r,s,t,v)=0}} C_{rstv} g_{rstv}(\mathbf{x}),$$

where C_{rstv} is a constant factor. In this work, C_{rstv} is generated procedurally by choosing for each (r, s, t, v) a value from a standard normal distribution (see the detailed discussion in [59]).

For each of the tesseract, tetrahedral prism, and pentatope elements, we have taken the quadrature rules of order \mathcal{P} and used them to estimate the integrals of polynomials f_{poly} of order p as follows

$$J = \sum_{i=1}^{N_p} \omega_i f_{\text{poly}}(\mathbf{x}_i).$$

For each monomial term, g_{rstv} , we can write the exact integral $I_{g_{rstv}}$ on an element as follows

$$I_{g_{rstv}} = \int_{\kappa} g_{rstv}(\mathbf{x}) d\mathbf{x} = \begin{cases} \frac{1}{(r+1)(s+1)(t+1)(v+1)} & \kappa \text{ is a tesseract} \\ \frac{s!t!v!}{(r+1)(s+t+v+3)!} & \kappa \text{ is a tetrahedral prism} \\ \frac{r!s!t!v!}{(r+s+t+v+4)!} & \kappa \text{ is a pentatope} \end{cases}$$

Thus, the exact integral of a polynomial that is being approximated by J can be given analytically by

$$J_{\infty}(\mathbf{x}; p) = \sum_{\substack{r+s+t+v \leq p \\ (r,s,t,v)=0}} C_{rstv} I_{g_{rstv}}.$$

In Figures 7, 8, and 9, the percent error produced by the quadrature rules on a single element, for each of the element types is shown as a function of the polynomial order p . In these plots, it can be seen that the quadrature rules guarantee exactness to machine precision for quadruple precision floating point numbers whenever $\mathcal{P} \geq p$, as we expect.

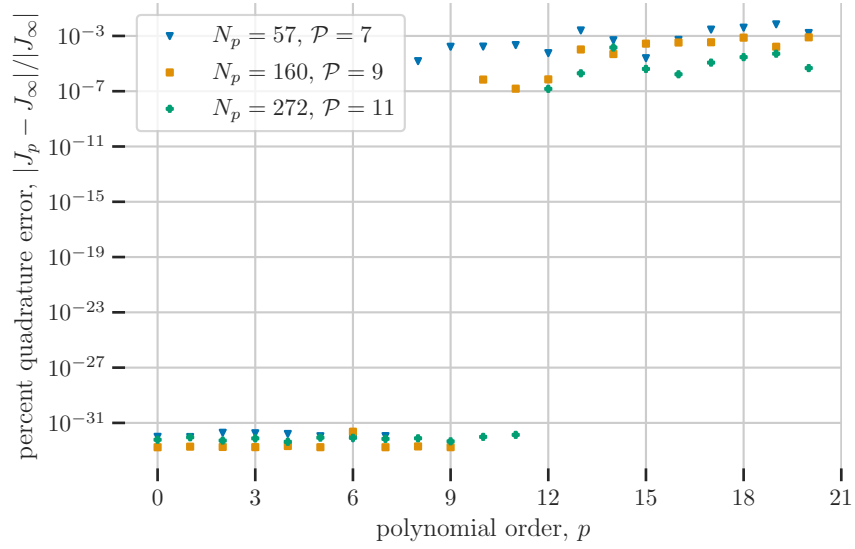


Figure 7: Percent error in polynomial integration on a tesseract element due to quadrature.

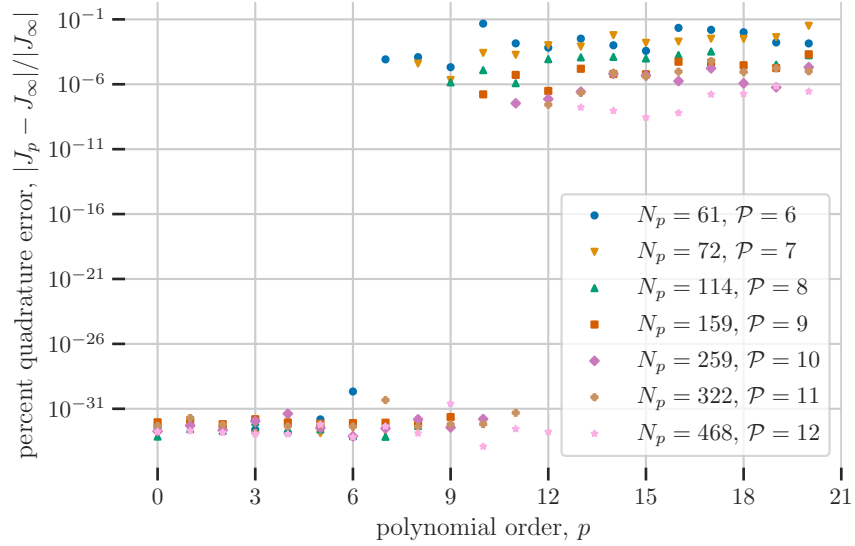


Figure 8: Percent error in polynomial integration on a tetrahedral prism element due to quadrature.

6.2 Integration of transcendental functions on multi-element grids

Next, we seek to quantify the performance of the quadrature rules in situations that are immediately relevant to finite element applications. We will

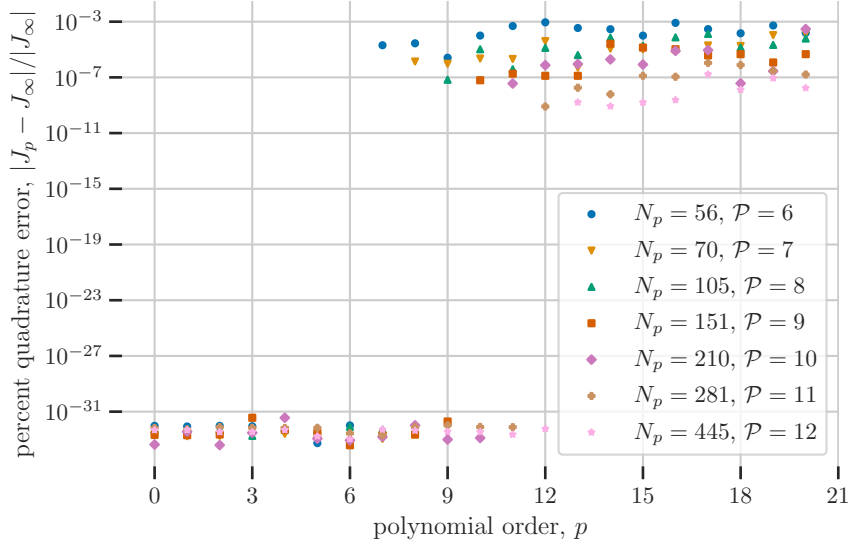


Figure 9: Percent error in polynomial integration on a pentatope element due to quadrature.

consider a domain $\Omega = [0, 1]^4$, which we will tessellate with three uniform triangulations of Ω : $\mathcal{T}_{\text{tesseract}}$, $\mathcal{T}_{\text{prism}}$, and $\mathcal{T}_{\text{pentatope}}$. For $\mathcal{T}_{\text{tesseract}}$, each dimension of the 4-cube domain is subdivided $m \in \{1, 2, 3, \dots, 12\}$ times, into $N_{\text{elem}} = m^4$ tesseract elements. In the case of the prismatic and pentatope grids, each tesseract element is further subdivided into either tetrahedral prisms or pentatopes by using the Kuhn-Freudenthal triangulation on the first three or all four dimensions of the tesseract element, respectively. This results in $N_{\text{elem}} = 3!m^4$ tetrahedral prism or $N_{\text{elem}} = 4!m^4$ pentatope elements respectively. In each of these three cases, the integral of a function $f \in L_1(\Omega)$ is then computed by

$$J_\infty = \int_{\Omega} f(\mathbf{x}) \, d\mathbf{x} \approx J \equiv \sum_{\kappa \in \mathcal{T}} \sum_{i=1}^{N_p} \omega_i^{(\kappa)} f(\mathbf{x}_i^{(\kappa)}),$$

where $\mathbf{x}_i^{(\kappa)}$ and $\omega_i^{(\kappa)}$ are transformed from the appropriate reference element to each physical element.

In order to understand the performance of the quadrature rules, we will evaluate their use on three transcendental functions, namely an exponential function:

$$f_1 = \exp(x^2 + 2y^3 + 3z^4 + 4t^5),$$

a sinusoidal function:

$$f_2 = \sin(x^2 + 2y^3 + 3z^4 + 4t^5),$$

and an even function (also sinusoidal):

$$f_3 = \sin(x^2 + y^2 + z^2 + t^2).$$

In Figures 10, 11, and 12, the percent error induced by the quadrature approximation for each function is plotted with respect to the grid characteristic length

$$h = \sqrt[4]{\frac{|\Omega|}{N_{\text{elem}}}},$$

with $|\Omega|$ the volume of the domain and N_{elem} the number of elements.

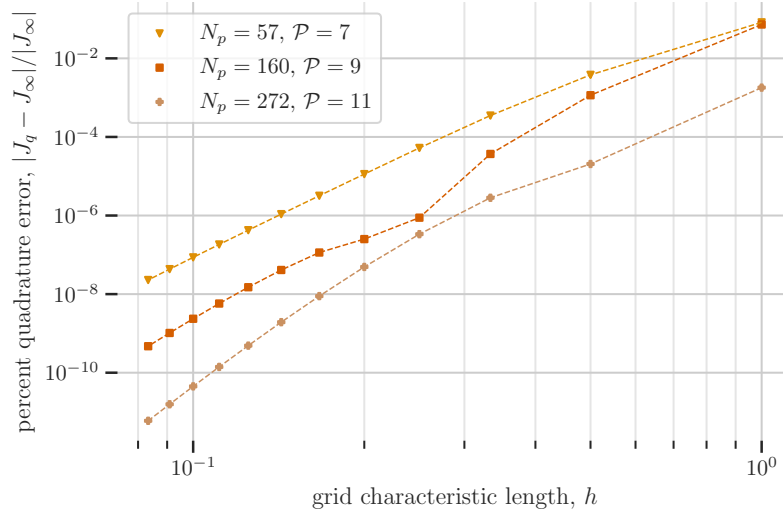


Figure 10: Percent error in integration of f_1 on a tesseract grid due to quadrature.

Similarly, in Figures 13, 14, and 15 we can see the results for the tetrahedral prism elements, and in Figures 16, 17, and 18, the results for the pentatope elements. The conclusion from these collected results is that quadrature error seems to be well behaved for each of the included transcendental functions, and approximations of integrals of similar functions by these quadrature rules can be expected to be accurate. In each case, quadrature rules of design order \mathcal{P} produce convergence rates that are at least $h^{\mathcal{P}}$ and frequently better ($h^{\mathcal{P}+1}$ or $h^{\mathcal{P}+2}$), which makes them well suited for finite element methods.

We note that, in a few cases lower degree rules outperform higher degree rules. This is likely due to a coincidental and beneficial alignment between the symmetry groups of a lower degree rule and the topology of one of our transcendental functions. Evidently, this trend will not hold for arbitrary transcendental functions, and the stronger quadrature rule will tend to outperform the weaker rule in most cases.

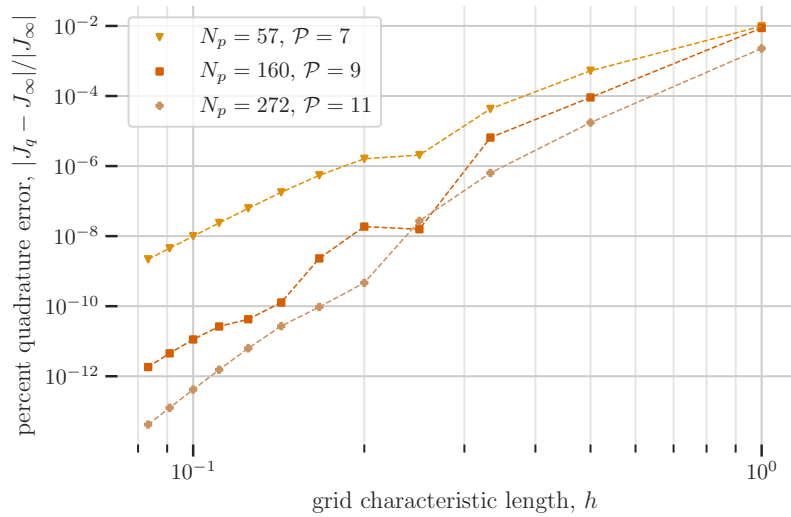


Figure 11: Percent error in integration of f_2 on a tesseract grid due to quadrature.

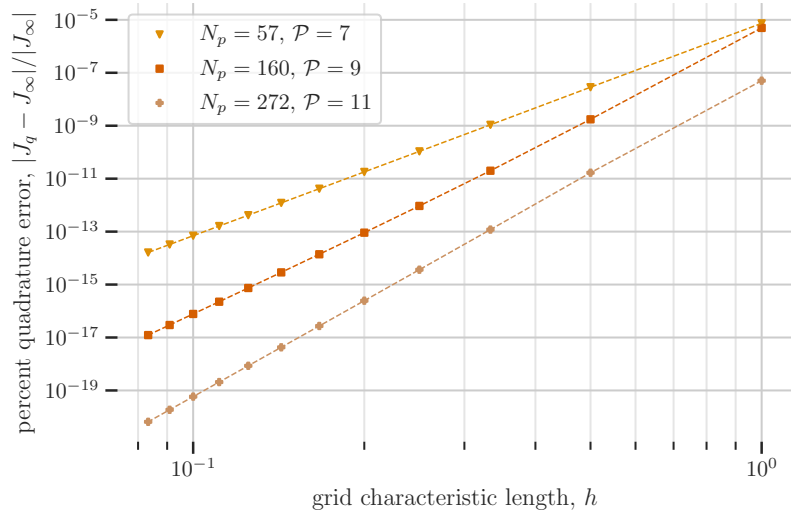


Figure 12: Percent error in integration of f_3 on a tesseract grid due to quadrature.

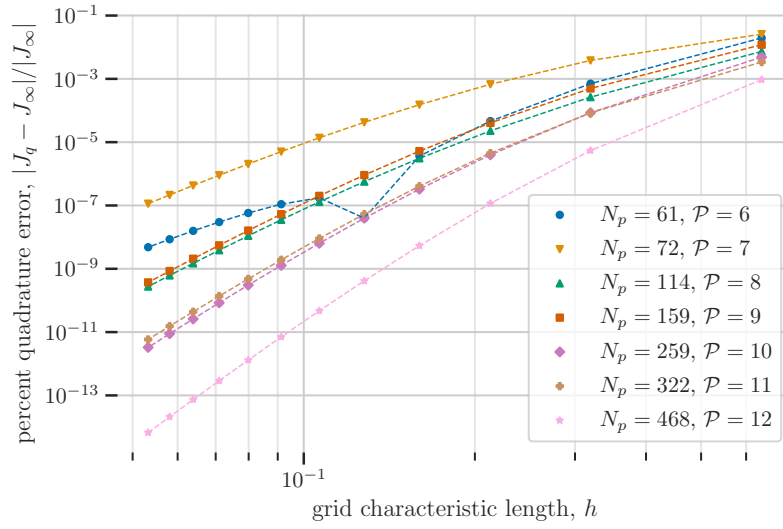


Figure 13: Percent error in integration of f_1 on a prismatic grid due to quadrature.

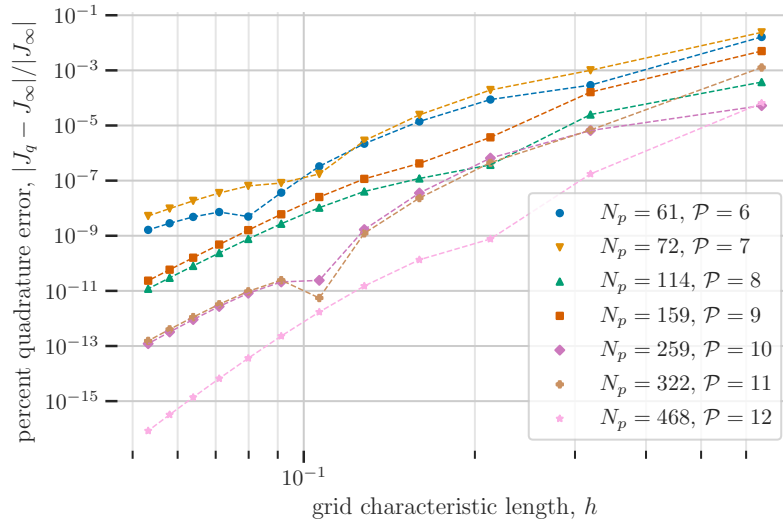


Figure 14: Percent error in integration of f_2 on a prismatic grid due to quadrature.

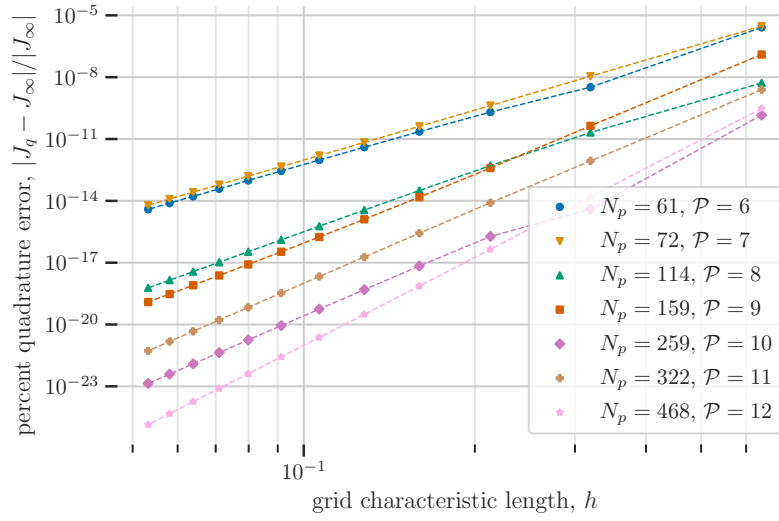


Figure 15: Percent error in integration of f_3 on a prismatic grid due to quadrature.

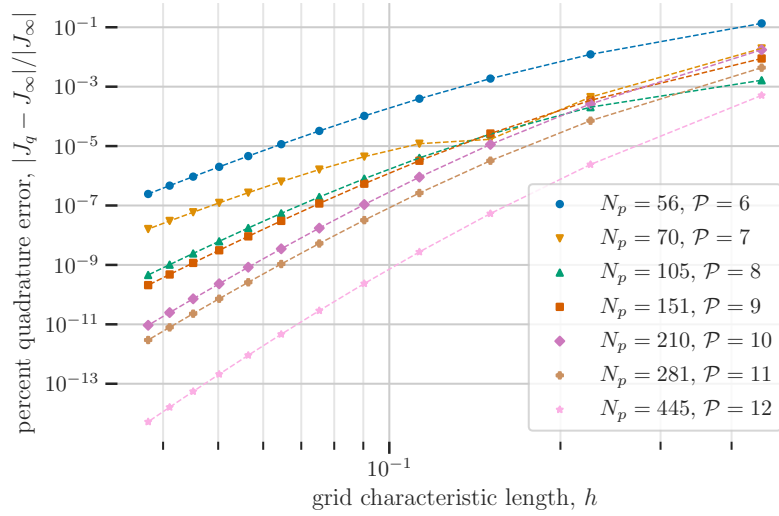


Figure 16: Percent error in integration of f_1 on a pentatope grid due to quadrature.

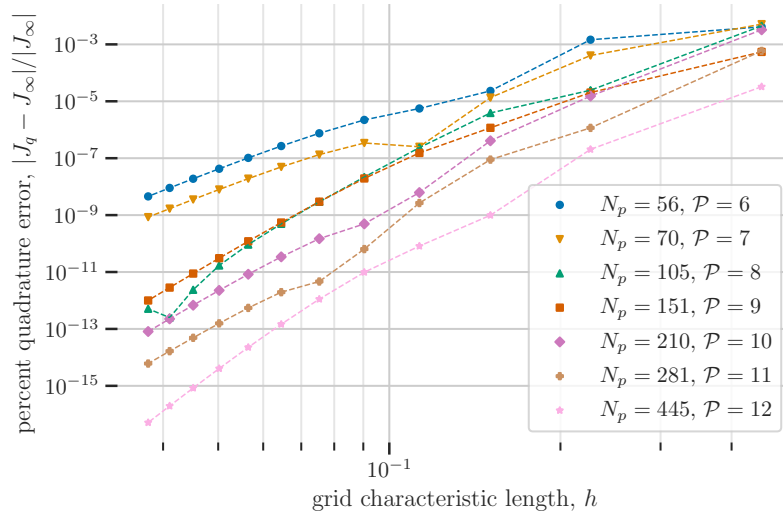


Figure 17: Percent error in integration of f_2 on a pentatope grid due to quadrature.

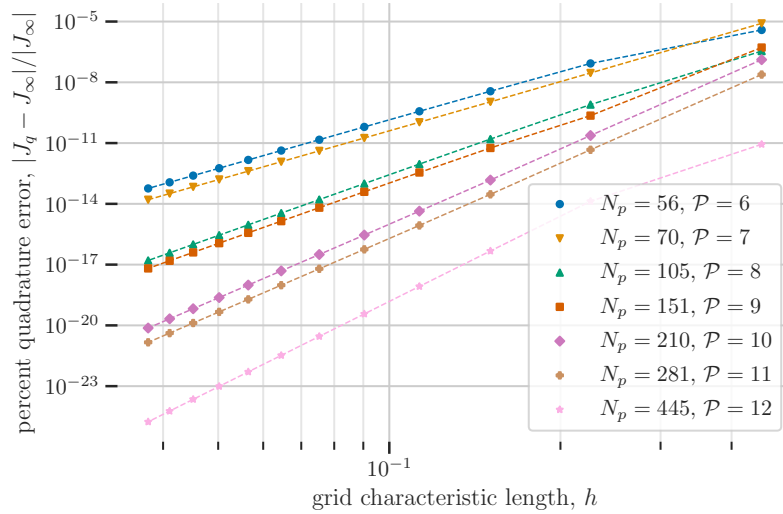


Figure 18: Percent error in integration of f_3 on a pentatope grid due to quadrature.

7. Conclusion

In this article, we have explored the numerical foundations of finite element methods for real-world $3d+t$ problems. We began our discussion by introducing a rigorous approach for generating four-dimensional elements using sequences of 0/1-polytopes. Thereafter, we demonstrated that at least one such sequence can be naturally encoded in terms of four digit binary numbers. Next, we narrowed our focus to consider the tesseract, tetrahedral prism, and pentatope elements. For each element type, we presented a brief review of the basic numerical properties, including explicit definitions of the reference domain, limits of integration, orthonormal polynomial basis, and symmetry groups. In addition, for each element, we constructed a new set of fully symmetric quadrature rules. Finally, we demonstrated the effectiveness of our quadrature rules by performing a detailed set of numerical experiments.

We anticipate that our work (above) will significantly encourage the development of *general* space-time methods for practical applications, and will not merely be limited to finite element methods. In particular, the newly developed element sequences will be useful in the construction of hybrid four-dimensional meshes for space-time visualization and data manipulation purposes. In addition, the newly developed quadrature rules will be immediately useful for both space-time finite element *and* finite volume methods.

Declaration of Competing Interests

The authors declare that they have no known competing financial interests or personal relationships that could have appeared to influence the work reported in this paper.

Acknowledgements

The authors would like to thank Dr. Chuluunbaatar Ochbadrakh for helping error-check the quadrature rules.

Funding

This research did not receive any specific grant from funding agencies in the public, commercial, or not-for-profit sectors.

References

- [1] A. Ern, J.-L. Guermond, *Theory and Practice of Finite Elements*, Vol. 159, Springer Science & Business Media, 2013.
- [2] C. Johnson, *Numerical Solution of Partial Differential Equations by the Finite Element Method*, Courier Corporation, 2012.
- [3] U. Langer, S. E. Moore, M. Neumüller, Space–time isogeometric analysis of parabolic evolution problems, *Computer Methods in Applied Mechanics and Engineering* 306 (2016) 342–363.
- [4] K. Takizawa, T. E. Tezduyar, T. Terahara, Ram-air parachute structural and fluid mechanics computations with the space–time isogeometric analysis (ST-IGA), *Computers & Fluids* 141 (2016) 191–200.
- [5] K. Takizawa, T. E. Tezduyar, Y. Otoguro, T. Terahara, T. Kuraishi, H. Hattori, Turbocharger flow computations with the space–time isogeometric analysis (ST-IGA), *Computers & Fluids* 142 (2017) 15–20.
- [6] Y. Otoguro, K. Takizawa, T. E. Tezduyar, Space–time VMS computational flow analysis with isogeometric discretization and a general-purpose NURBS mesh generation method, *Computers & Fluids* 158 (2017) 189–200.
- [7] K. Takizawa, T. E. Tezduyar, T. Terahara, T. Sasaki, Heart valve flow computation with the integrated space–time VMS, slip interface, topology change and isogeometric discretization methods, *Computers & Fluids* 158 (2017) 176–188.
- [8] K. Takizawa, T. E. Tezduyar, Y. Otoguro, Stabilization and discontinuity-capturing parameters for space–time flow computations with finite element and isogeometric discretizations, *Computational Mechanics* 62 (5) (2018) 1169–1186.
- [9] Y. Otoguro, K. Takizawa, T. E. Tezduyar, K. Nagaoka, S. Mei, Turbocharger turbine and exhaust manifold flow computation with the space–time variational multiscale method and isogeometric analysis, *Computers & Fluids* 179 (2019) 764–776.
- [10] U. Langer, S. Matculevich, S. Repin, Adaptive space-time isogeometric analysis for parabolic evolution problems, in: *Space–Time Methods: Applications to Partial Differential Equations*, edited by U. Langer and O. Steinbach, Radon Series on Computational and Applied Mathematics, Vol. 25, De Gruyter, 2019, pp. 141–184.
- [11] T. Terahara, K. Takizawa, T. E. Tezduyar, A. Tsushima, K. Shiozaki, Ventricle-valve-aorta flow analysis with the Space–Time Isogeometric Discretization and Topology Change, *Computational Mechanics* (2020) 1–21.
- [12] J. J. Van der Vegt, H. Van der Ven, Space–time discontinuous Galerkin finite element method with dynamic grid motion for inviscid compressible flows: I. General formulation, *Journal of Computational Physics* 182 (2) (2002) 546–585.
- [13] H. Van der Ven, J. J. van der Vegt, Space–time discontinuous Galerkin finite element method with dynamic grid motion for inviscid compressible flows: II. Efficient flux quadrature, *Computer Methods in Applied Mechanics and Engineering* 191 (41-42) (2002) 4747–4780.
- [14] C. M. Klaij, J. J. van der Vegt, H. van der Ven, Space–time discontinuous Galerkin method for the compressible Navier–Stokes equations, *Journal of Computational Physics* 217 (2) (2006) 589–611.
- [15] L. T. Diosady, S. M. Murman, Higher-order methods for compressible turbulent flows using entropy variables, in: *53rd AIAA Aerospace Sciences Meeting*, 2015.

- [16] L. T. Diosady, S. M. Murman, Tensor-product preconditioners for higher-order space–time discontinuous Galerkin methods, *Journal of Computational Physics* 330 (2017) 296–318.
- [17] L. T. Diosady, S. M. Murman, A linear-elasticity solver for higher-order space-time mesh deformation, in: 2018 AIAA Aerospace Sciences Meeting, 2018.
- [18] L. T. Diosady, S. M. Murman, Scalable tensor-product preconditioners for high-order finite-element methods: Scalar equations, *Journal of Computational Physics* 394 (2019) 759–776.
- [19] T. E. Tezduyar, S. Sathe, R. Keedy, K. Stein, Space–time finite element techniques for computation of fluid–structure interactions, *Computer Methods in Applied Mechanics and Engineering* 195 (17-18) (2006) 2002–2027.
- [20] T. E. Tezduyar, S. Sathe, Modelling of fluid–structure interactions with the space–time finite elements: Solution techniques, *International Journal for Numerical Methods in Fluids* 54 (6-8) (2007) 855–900.
- [21] T. E. Tezduyar, K. Takizawa, C. Moorman, S. Wright, J. Christopher, Space–time finite element computation of complex fluid–structure interactions, *International Journal for Numerical Methods in Fluids* 64 (10-12) (2010) 1201–1218.
- [22] T. E. Tezduyar, K. Takizawa, Space–time computations in practical engineering applications: a summary of the 25-year history, *Computational Mechanics* 63 (4) (2019) 747–753.
- [23] Z. Yang, F. Liu, Y. Nie, I. Turner, An unstructured mesh finite difference/finite element method for the three-dimensional time-space fractional Bloch-Torrey equations on irregular domains, *Journal of Computational Physics* 408 (2020) 109284.
- [24] M. Al-Smadi, A. Freihat, H. Khalil, S. Momani, R. Ali Khan, Numerical multistep approach for solving fractional partial differential equations, *International Journal of Computational Methods* 14 (03) (2017) 1750029.
- [25] M. Al-Smadi, O. A. Arqub, Computational algorithm for solving fredholm time-fractional partial integrodifferential equations of dirichlet functions type with error estimates, *Applied Mathematics and Computation* 342 (2019) 280–294.
- [26] M. Al-Smadi, O. A. Arqub, S. Hadid, An attractive analytical technique for coupled system of fractional partial differential equations in shallow water waves with conformable derivative, *Communications in Theoretical Physics* 72 (8) (2020) 085001.
- [27] M. Al-Smadi, O. A. Arqub, S. Momani, Numerical computations of coupled fractional resonant Schrödinger equations arising in quantum mechanics under conformable fractional derivative sense, *Physica Scripta* 95 (7) (2020) 075218.
- [28] G. E. Karniadakis, J. S. Hesthaven, I. Podlubny, Special Issue on “Fractional PDEs: Theory, Numerics, and Applications”, *Journal of Computational Physics* 293 (2015) 1–3.
- [29] E. Kharazmi, Z. Mao, G. Pang, M. Zayernouri, G. E. Karniadakis, Fractional calculus and numerical methods for fractional PDEs, in: *First Congress of Greek Mathematicians: Proceedings of the Congress held in Athens, Greece, June 25–30, 2018*, Walter de Gruyter, 2020, p. 91.
- [30] M. Behr, Simplex space–time meshes in finite element simulations, *International Journal for Numerical Methods in Fluids* 57 (9) (2008) 1421–1434.
- [31] V. Karyofylli, M. Frings, S. Elgeti, M. Behr, Simplex space-time meshes in two-phase flow simulations, *International Journal for Numerical Methods in Fluids* 86 (3) (2018) 218–230.

- [32] V. Karyofylli, L. Wendling, M. Make, N. Hosters, M. Behr, Simplex space-time meshes in thermally coupled two-phase flow simulations of mold filling, *Computers & Fluids* 192 (2019) 104261.
- [33] M. von Danwitz, V. Karyofylli, N. Hosters, M. Behr, Simplex space-time meshes in compressible flow simulations, *International Journal for Numerical Methods in Fluids* 91 (1) (2019) 29–48.
- [34] L. Wang, Discontinuous galerkin methods on moving domains with large deformations, Ph.D. thesis, University of California, Berkeley (2015).
- [35] C. Lehrenfeld, The Nitsche XFEM-DG space-time method and its implementation in three space dimensions, *SIAM Journal on Scientific Computing* 37 (1) (2015) A245–A270.
- [36] A. D. Mont, Adaptive unstructured spacetime meshing for four-dimensional spacetime discontinuous galerkin finite element methods, Master’s thesis, University of Illinois at Urbana-Champaign (2012).
- [37] A. Üngör, A. Sheffer, Tent-Pitcher: A meshing algorithm for space-time discontinuous Galerkin methods, in: In proc. 9th int’l. meshing roundtable, Citeseer, 2000, pp. 111–122.
- [38] M. Neumüller, O. Steinbach, Refinement of flexible space–time finite element meshes and discontinuous Galerkin methods, *Computing and Visualization in Science* 14 (5) (2011) 189–205.
- [39] M. Neumüller, Space-time methods: Fast solvers and applications, Ph.D. thesis, Graz University of Technology (2013).
- [40] P. Foteinos, N. Chrisochoides, 4d space–time Delaunay meshing for medical images, *Engineering with Computers* 31 (3) (2015) 499–511.
- [41] G. Belda-Ferrín, A. Gargallo-Peiró, X. Roca, Local bisection for conformal refinement of unstructured 4D simplicial meshes, in: *International Meshing Roundtable*, Springer, 2018, pp. 229–247.
- [42] P. C. Caplan, R. Haines, D. L. Darmofal, M. C. Galbraith, Anisotropic geometry-conforming d-simplicial meshing via isometric embeddings, *Procedia Engineering* 203 (2017) 141–153.
- [43] P. Caplan, R. Haines, D. Darmofal, M. Galbraith, Extension of local cavity operators to 3d+t space-time mesh adaptation, in: *AIAA Scitech 2019 Forum*, 2019.
- [44] P. C. Caplan, Four-dimensional anisotropic mesh adaptation for spacetime numerical simulations, Ph.D. thesis, Massachusetts Institute of Technology (2019).
- [45] P. C. Caplan, R. Haines, D. L. Darmofal, Four-dimensional anisotropic mesh adaptation, *Computer-Aided Design* (2020) 102915.
- [46] J. Proriol, Sur une famille de polynomes á deux variables orthogonaux dans un triangle, *Comptes Rendus Hebdomadaires des Seances de l Academie des Sciences* 245 (26) (1957) 2459–2461.
- [47] T. Koornwinder, Two-variable analogues of the classical orthogonal polynomials, in: *Theory and Application of Special Functions*, Elsevier, 1975, pp. 435–495.
- [48] M. Dubiner, Spectral methods on triangles and other domains, *Journal of Scientific Computing* 6 (4) (1991) 345–390.
- [49] R. G. Owens, Spectral approximations on the triangle, *Proceedings of the Royal Society of London. Series A: Mathematical, Physical and Engineering Sciences* 454 (1971) (1998) 857–872.

- [50] J. S. Hesthaven, T. Warburton, Nodal discontinuous Galerkin methods: Algorithms, analysis, and applications, Springer Science & Business Media, 2007.
- [51] G. Karniadakis, S. Sherwin, Spectral/hp Element Methods for Computational Fluid Dynamics, Oxford University Press, 2013.
- [52] T. J. Hughes, The Finite Element Method: Linear Static and Dynamic Finite Element Analysis, Courier Corporation, 2012.
- [53] T. Warburton, J. S. Hesthaven, On the constants in hp-finite element trace inverse inequalities, *Computer Methods in Applied Mechanics and Engineering* 192 (25) (2003) 2765–2773.
- [54] A. H. Stroud, Approximate Calculation of Multiple Integrals, Prentice-Hall, 1971.
- [55] T. Sørveik, T. O. Espelid, Fully symmetric integration rules for the 4-cube, Tech. rep., University of Bergen, Norway (1987).
- [56] C. Majorana, S. Odorizzi, R. Vitaliani, Shortened quadrature rules for finite elements, *Advances in Engineering Software* 4 (2) (1982) 52–57.
- [57] T. Sørveik, T. O. Espelid, Fully symmetric integration rules for the 4-cube, *BIT Numerical Mathematics* 29 (1) (1989) 148–153.
- [58] T. Sørveik, Reliable and efficient adaptive quadrature algorithms, Ph.D. thesis, University of Bergen, Norway (1988).
- [59] D. M. Williams, C. V. Frontin, E. A. Miller, D. L. Darmofal, A family of symmetric, optimized quadrature rules for pentatopes, *Computers & Mathematics with Applications* 80 (5) (2020) 1405–1420.
- [60] P. C. Hammer, A. H. Stroud, Numerical integration over simplexes, *Mathematical Tables and Other Aids to Computation* 10 (55) (1956) 137–139.
- [61] A. Stroud, Some approximate integration formulas of degree 3 for an n-dimensional simplex, *Numerische Mathematik* 9 (1) (1966) 38–45.
- [62] A. A. Gusev, V. P. Gerdt, O. Chuluunbaatar, G. Chuluunbaatar, S. I. Vinitzky, V. Derbov, A. Gózdź, P. Krassovitskiy, Symbolic-numerical algorithms for solving elliptic boundary-value problems using multivariate simplex lagrange elements, in: *International Workshop on Computer Algebra in Scientific Computing*, Springer, 2018, pp. 197–213.
- [63] G. M. Ziegler, Lectures on 0/1-polytopes, in: *Polytopes—Combinatorics and Computation (Oberwolfach, 1997)*, Vol. 29 of DMV Sem., Birkhäuser, Basel, 2000, pp. 1–41.
- [64] O. Aichholzer, Extremal properties of 0/1-polytopes of dimension 5, in: *Polytopes—Combinatorics and Computation (Oberwolfach, 1997)*, Vol. 29 of DMV Sem., Birkhäuser, Basel, 2000, pp. 111–130.
- [65] B. Baumeister, C. Haase, B. Nill, A. Paffenholz, On permutation polytopes, *Advances in Mathematics* 222 (2009) 431–452.
- [66] A. Cihangir, On 0/1-polytopes with nonobtuse triangulations, *Applied Mathematics and Computation* 267 (2015) 17–27.
- [67] B. Grünbaum, Convex polytopes, 2nd Edition, Vol. 221 of Graduate Texts in Mathematics, Springer-Verlag, New York, 2003.
- [68] C. Zong, What is known about unit cubes?, *Bulletin of the American Mathematical Society* 42 (2) (2005) 181–211.

- [69] F. D. Witherden, P. E. Vincent, On the identification of symmetric quadrature rules for finite element methods, *Computers & Mathematics with Applications* 69 (10) (2015) 1232–1241.
- [70] J. Maeztu, E. Sáinz de La Maza, Consistent structures of invariant quadrature rules for the n -simplex, *Mathematics of Computation* 64 (211) (1995) 1171–1192.
- [71] S. A. Orszag, Spectral methods for problems in complex geometrics, in: *Numerical Methods for Partial Differential Equations*, Elsevier, 1979, pp. 273–305.
- [72] M. G. Duffy, Quadrature over a pyramid or cube of integrands with a singularity at a vertex, *SIAM Journal on Numerical Analysis* 19 (6) (1982) 1260–1262.